Rule-Driven Defect Detection in CT Images of Hardwood Logs

Erol Sarigul[a], A. Lynn Abbott[b], Daniel L. Schmoldt[c]

[a] *Bradley Department of Electrical Engineering, Virginia Tech, Blacksburg, Virginia 24061 USA, esarigul@vt.edu*
[b] *Bradley Department of Electrical Engineering, Virginia Tech, Blacksburg, Virginia 24061 USA, abbott@vt.edu*
[c] *USDA Forest Service, Biological Systems Engineering Dept., 460 Henry Mall, University of Wisconsin, Madison, Wisconsin 53706 USA, dlschmol@facstaff.wisc.edu*

Abstract

This paper deals with automated detection and identification of internal defects in hardwood logs using computed tomography (CT) images. We have developed a system that employs artificial neural networks to perform tentative classification of logs on a pixel-by-pixel basis. This approach achieves a high level of classification accuracy for several hardwood species (northern red oak, *Quercus rubra*, L., water oak, *Q. nigra*, L., yellow poplar, *Liriodendron tulipifera*, L., and black cherry, *Prunus serotina*, Ehrh.), and three common defect types (knots, splits, and decay). Although the results are very satisfactory statistically, a subjective examination reveals situations that could be refined in a subsequent post-processing step. We are currently developing a rule-based approach to region refinement to augment the initial emphasis on local information. The resulting rules are domain dependent, utilizing information that depends on region shape and type of defect. For example, splits tend to be long and narrow, and this knowledge can be used to merge smaller, disjoint regions that have tentatively been labeled as splits. Similarly, image regions that represent knots, decay, and clear wood can be refined by removing small, spurious points and by smoothing the boundaries of these regions. Mathematical morphology operators can be used for most of these tasks. This paper provides details concerning the domain-dependent rules by which morphology operators are chosen, and for merging results from different operations.

Keywords: Rule-Based Analysis; Morphological Image Processing; Defect Detection; Wood Processing

Introduction

The commercial value of hardwood lumber is inversely related to the quantity and sizes of defects that are present. For this reason, each log should be sawn so that defects are reduced in the resulting boards. Traditionally, however, saw operators convert logs to boards using only visible cues from log surfaces. Without complete knowledge of internal defect types and locations, it is not possible to improve log breakdown significantly.

Computed tomography (CT) scanning has been studied as a means of providing internal defect information (e.g., Benson-Coopers *et al*. 1982, Hopkins *et al*. 1982, Cown and Clement 1983, Taylor *et al*. 1984, Burgess 1985, Birkeland and Holoyen 1987, Chang *et al*. 1989, Wagner *et al*. 1989, Hodges *et al*. 1990, Harless *et al*. 1991, Occeña 1991, Davis and Wells 1992, Grönlund 1992, Grundberg and Grönlund 1992, Zhu 1993, Schmoldt 1996). Researchers have employed a variety of methods to detect and identify defects in CT images. For example, several studies have shown good results using artificial neural network (ANN) classifiers (Li *et al*. 1996, Schmoldt *et al*. 1997, Schmoldt *et al*. 2000). However, the problem is difficult because of the inherently variability of wood, and complete success has not yet been achieved.

This paper reports work that is in progress to *improve* the results that are produced by an existing defect-detection system. Initial classification is performed using local neighborhoods of CT density values. These serve as input values to an ANN, which assigns a label ("knot," "decay," "split", "bark," or "clear wood") to each pixel in the image. The post-processing module that is described here uses higher-level, domain-dependent knowledge to refine initial classification results. There are several motivations for such an approach. First, the initial ANN-based classifier depends primarily on information from very small image neighborhoods, and identifies defects on a pixel-by-pixel basis. It therefore ignores such information such as defect shape, size, and position within the log. Second, the rule-based post-processing approach that we describe here can employ fundamentally different types of rules for different defects, whereas the ANN approach that we use is restricted to a single topology for all classes that it can identify. Finally, in some cases the ANN classifier yields results that are very good in a statistical sense, but a subjective evaluation reveals a need for additional refinement. For example, small spurious defect regions may have only a small effect on pixel-wise statistical classification accuracy, but are objectionable to the human observer. In many cases, such regions can be identified and eliminated easily.

The refined system depends heavily on the tools of mathematical morphology for post-processing. The basics of this are briefly presented in the next section of this paper. As shown in Figure 1, which illustrates the overall post-processing approach, different operations are applied to the different defect types that are detected by the ANN. The next 3 sections of this paper illustrate the application of morphology operators to the refinement of bark, knot, and split regions, respectively. The last sections briefly describe the refinement of other region types, and the integration of all post-processing results.

Overview of mathematical morphology

Mathematical morphology, also known as image algebra, is the study of shape or form using the concepts of set theory (Matheron 1975, Serra 1982, Haralick 1987). Mathematical morphology operations can be used to modify image shapes, reduce noise, and detect features of interest.

In this paper, we consider only binary images and binary morphology. In this case, only two different pixel values are possible, often called "foreground" and "background" levels. It is possible to represent a binary image as a set of (row, column) coordinate locations for all of the foreground points. Most morphology operations involve a *structuring element*, which is another set of (row, column) pairs. The structuring element is typically quite small, and its shape has a direct impact on the results.

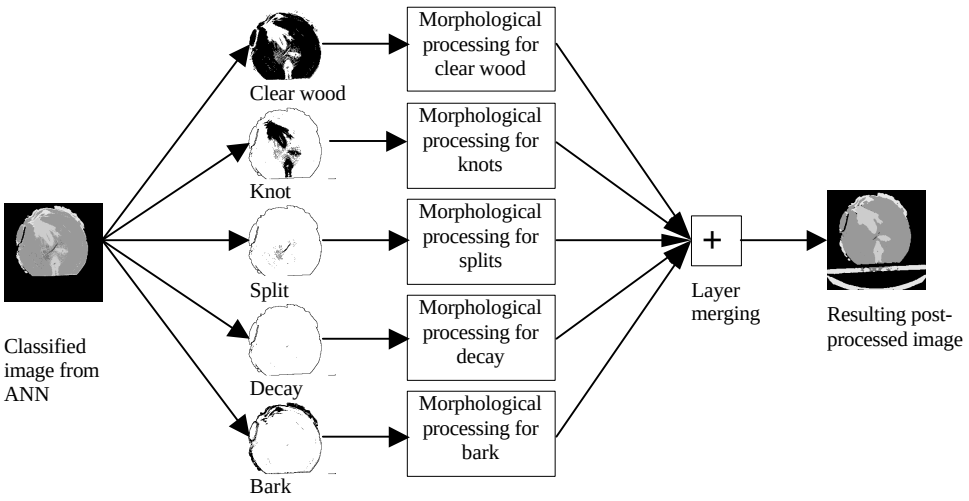

Figure 1. *Overview of rule-based post-processing approach. An artificial neural network assigns tentative labels to all wood pixels in a CT image. Each set of labels can be treated as a separate binary image, to be processed independently using morphological transformations. The individual results are merged to produce the final result.*

In the following discussion, it will be convenient to use subscript notation to represent the *translation* of a set:

$$(A)_x = \{a + x \mid a \in A\} . \tag{1}$$

Two fundamental operations of mathematical morphology are *dilation* and *erosion*. Intuitively, these operations tend to enlarge and reduce (respectively) the sizes of foreground regions in images. Let set A represent a binary image, and let B represent a structuring element. A definition of dilation is

$$A \oplus B = \{a + b \mid a \in A \text{ and } b \in B\} \tag{2}$$

and a definition of erosion is

$$A \ominus B = \{x \mid (B)_x \subseteq A\} . \tag{3}$$

The successive application of these two operations is common. The morphological *opening* of A by B is defined as

$$A \circ B = (A \ominus B) \oplus B \tag{4}$$

and *closing* is given by

$$A \bullet B = (A \oplus B) \ominus B . \tag{5}$$

A few other terms will also be needed later in the paper. The *complement* of a set can be written as

$$A^C = \{x \mid x \notin A\} . \tag{6}$$

The *reflection* of B, denoted $\hat{B}$, is defined as

$$\hat{B} = \{x \mid x = -b, b \in B\} . \tag{7}$$

The *Minkowski difference* of two sets A and B is defined as

$$A \setminus B = \{x \mid x \in A \text{ and } x \notin B\} = A \cap B^C \ . \tag{8}$$

Post-processing bark regions

In order to show how domain-dependent rules can be developed and applied, we begin with an example concerning bark. It is easy for the ANN to incorrectly label pixels as bark, as its density is very similar to that of clear wood. Because bark typically lies on the outside of a log (we ignore the case of included bark for the present), it is possible to state this simple rule: Retain only those bark regions in the image that lie at the outer boundary of the log. The high-level processing strategy is first to determine which points lie on the outside edge of the log, and then to retain only those bark regions that overlap one or more boundary points.

Let us first consider morphological post-processing operations that can be used to obtain the boundary. This is illustrated in Figure 2. Figure 2a shows an image of a red oak log that has lost most of its bark, except for the upper right and lower left portions of the image. A binary log image, in which (black) foreground points represent the log, is obtained as the union of all labeled images produced by the ANN (Figure 2b). This binary image is dilated using a 3×3 structuring element, and points associated with Figure 2b are removed from the dilated version. The result is a representation of the log's boundary, as shown in Figure 2c, and will be used in subsequent processing. Algebraically, the procedure can be written as

$$C = (A \oplus B) \setminus A = (A \oplus B) \cap A^c \tag{9}$$

where A is the binary log image, B is the structuring element, and C is the result. Notice that the structuring element can be expressed formally as B = {(-1, -1), (-1, 0), (-1, 1), (0, -1), (0, 0), (0, 1),(1, -1), (1, 0), (1, 1)}. Dilation by this structuring element causes A to be enlarged by one pixel in every direction.

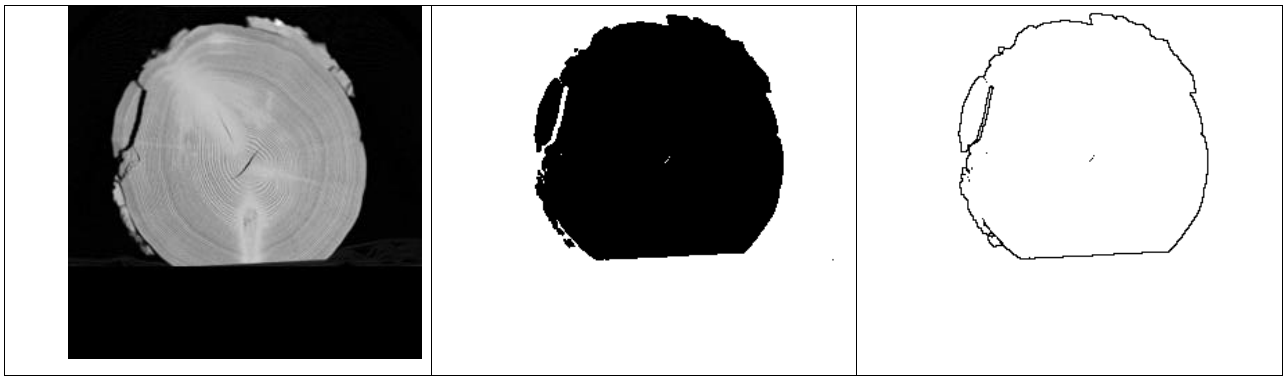

(a) (b) (c)

Figure 2. *Post-processing example for bark. (a) CT image slice of red oak log. (b) Foreground points associated with the log. (c) The detected outside boundary of the log.*

The next step is to eliminate regions detected by the ANN that do not touch the boundary. Initial bark regions for this image, as labeled by the ANN, are shown in Figure 3a. In this example, several small regions have been incorrectly labeled as bark, and a fairly large region near the top has also been incorrectly labeled. We first apply morphological opening to the initial bark region, using the same structuring element that is used in the extraction of the log's boundary. This removes small "necks" that

connect larger regions, smoothes region boundaries, and additionally removes some of the smaller spurious regions from further consideration. The result is shown in Figure 3b.

To this image we apply *conditional dilation*. This is an iterative procedure that retains only those regions that are designated initially using "marker" points. In our case all foreground points in the boundary image C (Figure 2c) serve as marker points. C is repeatedly dilated using the 3 × 3 structuring element B that was described earlier, but at every iteration the intermediate result is intersected with the bark image given in Figure 3b. We designate this input bark image as I_{bark}, and it serves formally as a "mask" image for the conditional dilation. The conditional dilation can be expressed as

$$I_{bark\_new} = (C \oplus B)^{(i)} \cap I_{bark} \tag{10}$$

where the superscript (i) represents the repetition index. The dilations and intersections continue until no change occurs; i.e., $(C \oplus B)^{(i)} \cap I_{bark} = (C \oplus B)^{(i+1)} \cap I_{bark}$. The result of this is shown in Figure 3c.

(a) (b) (c)

Figure 3. *Continued processing for bark. (a) Bark image. The dark points represent bark, as tentatively identified by the ANN. (b) The result of morphological opening. (c) The result after removing regions not on the boundary of the log.*

The post-processing steps for bark are summarized in the diagram of Figure 4.

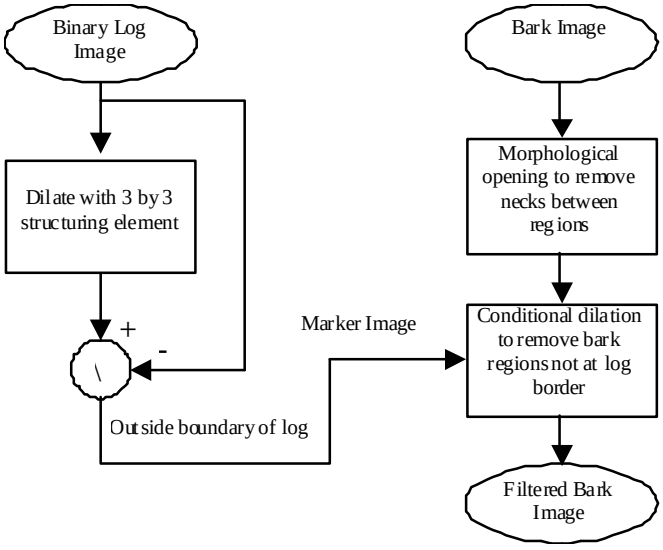

Figure 4. *Post-processing of bark regions. Relatively simple morphological processing leads to improved results.*

Post-processing knot regions

Knots are perhaps the most common type of defect in wood. Knots typically have a higher density than surrounding clear wood, and tend to have an rounded shape in images. (This is unlike splits, discussed in the next section, which tend to be long and narrow.) A problem with knots, and more generally with all defect detection in hardwoods, is that annual rings often cause misclassifications partly because of their wide variations in density. In addition, the ANN often classifies isolated high-density points as knots, and these need to be removed. This is shown in the example knot image of Figure 5.

(a) (b) (c)

Figure 5. *The result of morphological post-processing for knots. (a) Tentative knot image, as produced by the ANN classifier. The misclassifications shown here are perhaps worse than our typical classification cases, but serve to illustrate the efficacy of the post-processing approach. (b) Removal of isolated knot pixels. (c) Output produced by majority filtering.*

One method of removing isolated pixels is to use a morphological template-matching process known as the *hit-or-miss transform*. This operation requires specifying 2 different nonoverlapping structuring elements. One of them, B_1, specifies relative positions of foreground points to be matched, and the other, B_2, specifies relative positions of background points to be matched. The two structuring elements must satisfy $B_1 \cap B_2 = \varnothing$, and the hit-or-miss transform is defined as

$$A \otimes \{B_1, B_2\} = (A \ominus B_1) \cap (A^c \ominus B_2) . \tag{11}$$

Example structuring elements are shown in Figure 6, and the result of applying this transform to the image of Figure 5a is shown in Figure 5b.

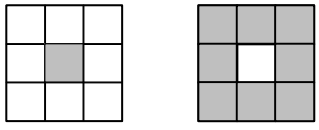

B_1 B_2

Figure 6. *Structuring elements for isolated pixel removal. B_1 is just a single point, and is the "hit" structuring element. B_2 consists of 8 points surrounding the center pixel, and is the "miss" structuring element.*

The hit-or-miss transform finds isolated points, and we wish to remove them from the image. This can be done by applying the following morphological operation,

$$I_{knot\_new} = I_{knot} \setminus \left(I_{knot} \otimes \{B_1, B_2\}\right) \ , \tag{12}$$

where I_{knot_new} is the filtered image, I_{knot} is the unfiltered image, and B_1, B_2 are structuring elements described above.

The *majority* algorithm is now used to connect isolated regions in a knot. The majority algorithm considers the 9 pixels within a 3×3 neighborhood. Because pixels can have only foreground or background values, more than half of the 9 pixels must have one of these two values. That value replaces the value at the center pixel. This was applied to the image in Figure 5b, resulting in Figure 5c.

Post-processing split regions

A split is a longitudinal and radial separation of the wood, due to the tearing apart of wood cells. Wood is distinctly anisotropic, meaning that its principal characteristics are different depending on direction. Post-processing operations can be selected to take advantage of the narrow, elongated shapes that are expected of split regions.

The flowchart procedure for this is given in Figure 7. First, a majority filter is applied (as described in the previous section) to partially eliminate problems due to annual rings. Next, morphology operations are employed to extract a *skeleton* of each region. A skeleton is a thinned representation of a region that retains information associated with its original size, orientation, and connectivity. Lantuéjoul (1980) showed that the skeleton of a binary image *A* could be expressed in terms of morphological erosions and openings. With *S*(*A*) denoting the skeleton of *A*, it can be shown that

$$S(A) = \bigcup_{k=0}^{K} S_k(A) \tag{13}$$

with

$$S_k(A) = \bigcup_{k=0}^{K} \{(A \Theta kB) \setminus [(A \Theta kB) \circ B]\} \tag{14}$$

where *B* is a structuring element, $(A \Theta kB)$ indicates *k* successive erosions of *A*, i.e.,

$$(A \Theta kB) = ((\cdots(A \Theta B) \Theta B) \Theta \cdots) \Theta B \quad , \tag{15}$$

and *K* is the number of steps before *A* erodes to an empty set:

$$K = \max \{k \mid (A \Theta kB) \neq \varnothing\} . \tag{16}$$

The skeletonization procedure will typically produce a thinned image in which some small, spurious regions remain. We now remove these, eliminating all regions having an area that is smaller than an empirically chosen threshold.

Because splits are very narrow, they are often difficult to detect in CT images. Because of this, splits are often detected by the ANN as separate regions that need to be linked. For the case that 2 or more split regions are present, we now apply a linking step that searches for skeleton endpoints that lie in close proximity. If the distance is sufficiently small between any two endpoints from different skeletons, then these two endpoints are joined by a straight line.

It is relatively simple to find the endpoints of skeletons, using morphological hit-or-miss operations with the different templates depicted in Figure 8. Each template represents a particular type of endpoint configuration using different sets, B_1 and B_2, as introduced in equation (11).

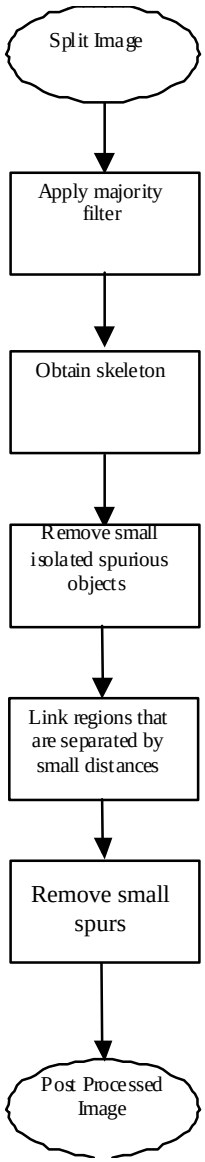

Figure 7. *Post-processing procedure for split regions. Because splits are often very narrow, they can be difficult to detect in CT images.*

After linking nearby skeletons, we refine the resulting regions by applying a morphological *pruning* algorithm to remove small, spurious branches. Conceptually, this is accomplished by repeatedly detecting skeleton endpoints and removing those endpoints. However, if this is performed directly, the main branches of the skeletons will be shortened as the small spurs are removed. To avoid this problem, we have adopted a skeleton filtering procedure introduced by Soille (1998). With this technique, spurious branches are removed without shortening the main branches that represent splits.

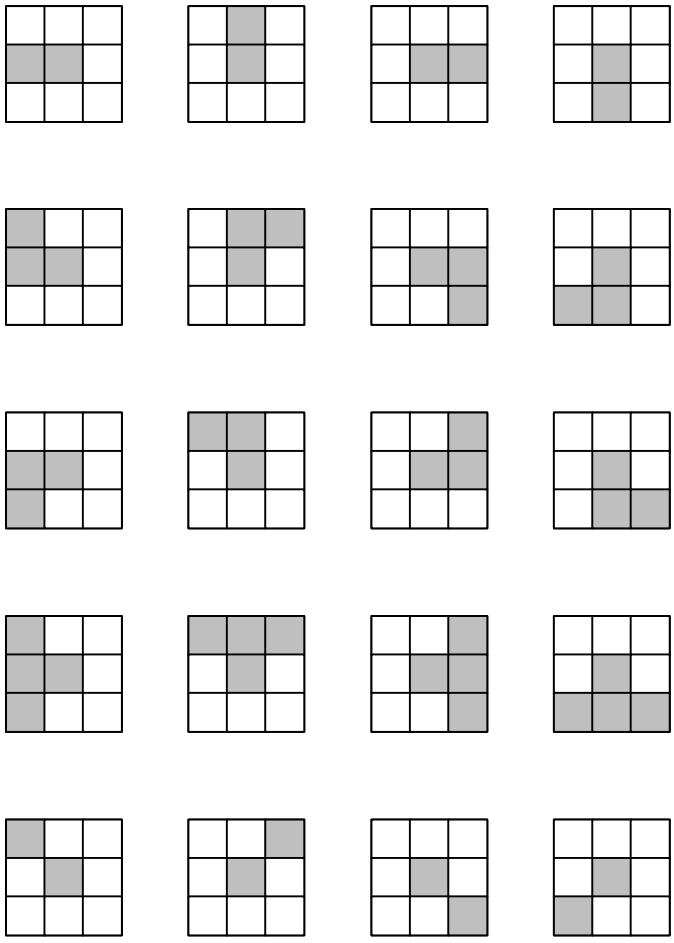

Figure 8. S*tructuring elements for endpoint detection. Each grid of 9 points represents a pair of structuring elements. In each case, the dark cells represent the set of foreground pixels (B_1 in equation (11)), and the white cells represent the set of background pixels (B_2).*

An example of split post-processing is illustrated in Figures 9 and 10. The CT image shown in Figure 9 contains a relatively long split. As Figure 10a illustrates, annual rings can confuse the ANN classifier in some cases. The majority-filtering algorithm eliminates most annual rings (Figure 10b), and skeletonization thins all of the resulting regions to 1-pixel widths (Figure 10c). Small regions are then removed (Figure 10d), and the remaining connected components are linked (Figure 10e). Finally, most spurious branches are removed from the resulting split region, while keeping the main branch unchanged. In this case, the result is not perfect; a connected side split (barely visible at the 2 o'clock position in Figure 9 and Figure 10a) is eventually eliminated by these post-processing steps. It is a sub-pixel resolution split that is difficult even for the human eye to detect.

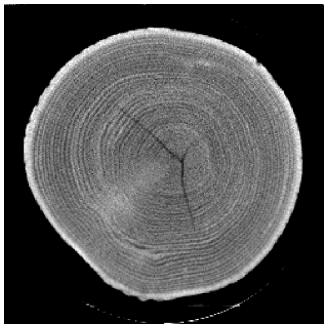

Figure 9. *An original CT image of red oak that contains a prominent split.*

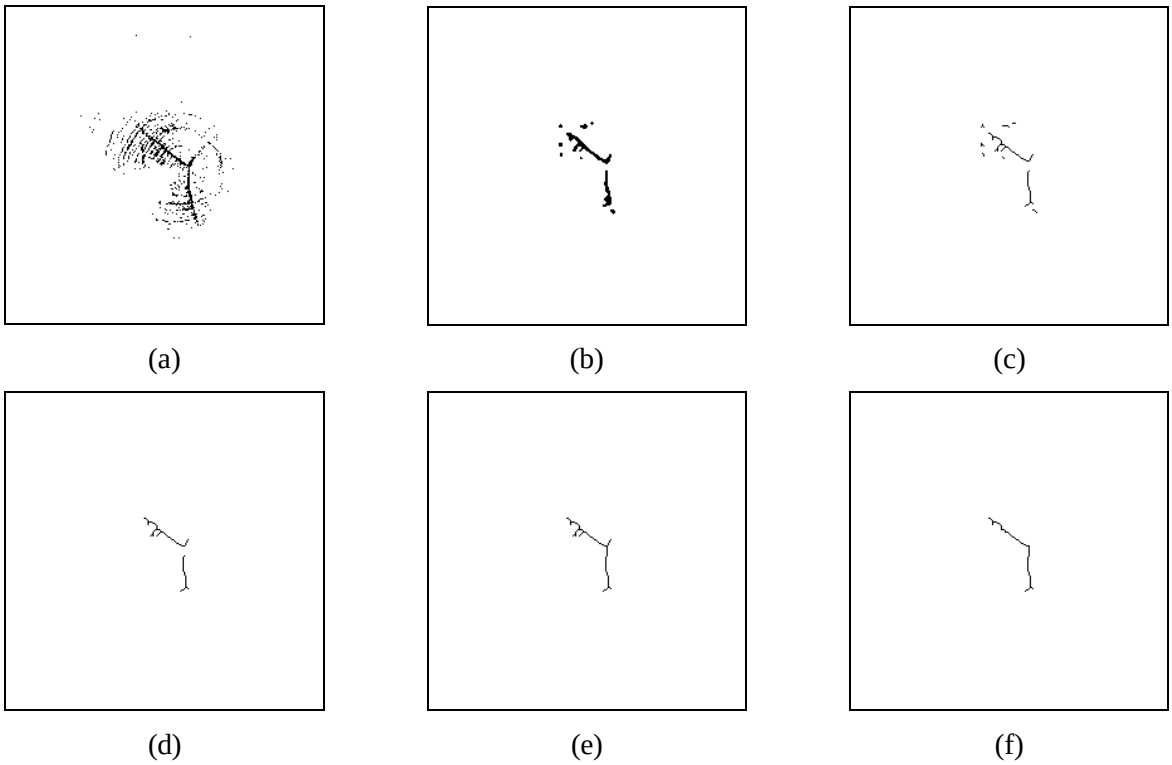

Figure 10. *Post-processing of split regions. (a) Split pixels, as tentatively assigned by the ANN. (b) The result of majority filtering algorithm. (c) Result of skeletonization. (d) Result of spurious object removal. (e) Result of branch linking. (f) Result of final skeleton filtering.*

Post-processing other region types

Clear wood and decay have similar geometric features, but they have very different density and texture characteristics, which the ANN can accurately distinguish in most cases. However, after removing spurious pixels and regions from each defect layer, the clear wood layer needs to be expanded to fill those vacated pixels. We use a *hole-filling* algorithm implemented using morphological operators. This algorithm inserts new foreground pixels into the clear wood layer, at points corresponding to the

surroundings of foreground regions in each defect layer. Because decay defects are so similar to clear wood, we apply a similar hole-filling algorithm to the decay defect layer.

Merging the results

After post-processing the individual layers separately (knots, splits, bark, and decay, and clear wood), we need to combine all separated layers into a final image. However, some defect regions will have grown, causing some regions from different layers to overlap. To resolve those overlaps, we have developed precedence rules (Table 1) to determine which defect label is retained when a pixel is assigned different labels by separate post-processing steps. For example, the region-filling algorithm applied to clear wood will create overlaps with knot regions. Because it is important to distinguish knots, we give those regions preference over clear wood regions. Whenever clear wood overlaps with any defect type, clear wood surrenders its pixel label at that specific point. Because splits and decay can appear inside of knot, they are given precedence over knots whenever an overlap occurs. Included bark has not been addressed by the current system, so bark assumes the highest precedence.

Table 1. *Precedence rules to resolve pairs of overlapping labels. The unshaded labels in the table represent the "winners" for cases that two labels (one shaded label from the left, and one shaded label from the bottom) have been assigned to a single pixel.*

Knot	Knot			
Split	Split	Split		
Decay	Decay	Knot	Split	
Bark	Bark	Bark	Bark	Bark
	Clear Wood	Knot	Split	Decay

An example of merging the result is shown in Figure 11. Using the original image given in Figure 2a, the background is detected and an ANN assigns tentative labels, as shown in Figure 11b. Morphological post-processing is conducted separately for each label type. The individual results are combined in Figure 11c. Subjectively, post-processing results in a considerable improvement for this example.

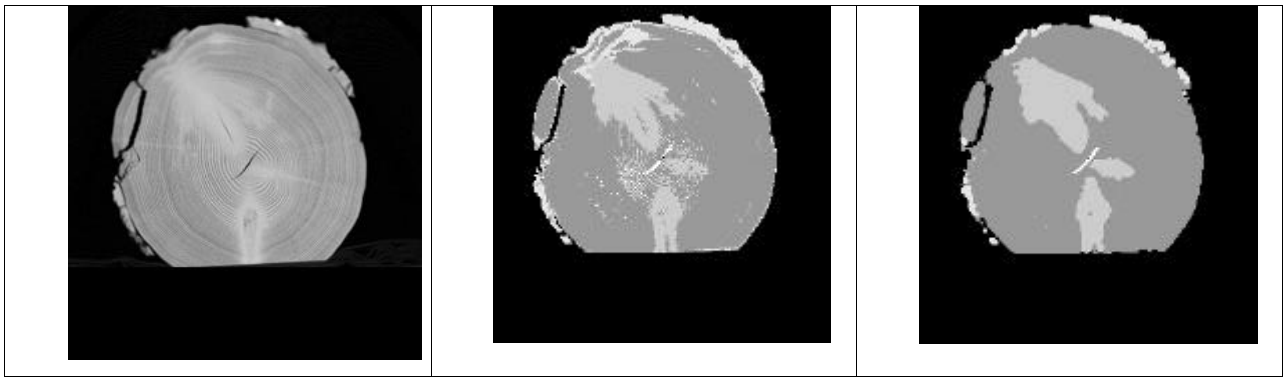

(a) (b) (c)

Figure 11. *Example to illustrate the improvements that can result from post-processing. (a) Original CT image, repeated from Figure 2a. (b) Initial labels assigned by ANN. (c) Combined result of post-processing. The split near the center has been enlarged slightly (by morphological dilation) to make it easier to see.*

Conclusions

Despite our success with ANNs for defect classification, spurious pixel misclassifications often remain from initial labeling. A wealth of powerful and effective morphological operators exist that can be used in combination based on domain-specific rules. These rules are tied to intuitive knowledge regarding defect manifestations within hardwood logs. Our current results with knots, bark, and split regions demonstrate impressive visual successes. However, we do not yet have quantitative estimates of misclassification improvements from post-processing.

The work reported here is one aspect of classification post-processing. We expect that there will be instances where small regions will remain following morphological post-processing. Other rule bases will need to be developed to handle those cases. Furthermore, the precedence rules in Table 1 can be extended to infer new defect types based on regional features. For example, if a knot pixel overlaps with a decay pixel, then the region containing those pixels could reasonably be labeled as an *unsound* knot. Otherwise, this defect type is not explicitly considered by either the ANN or the current binary morphology scheme. However, our approach separates post-processing into manageable and less-complex images that can be extensively manipulated and then combined into a composite representation of a log's internal features. This appears to be an effective and powerful approach to post-processing for defect detection.

Acknowledgement

This work was supported in part by USDA National Research Initiative competitive grant #98-35504-6581.

References

Benson-Cooper, D. M., Knowles, R. L., Thomson, F. J., and Cown, D.J., 1982. Computed tomographic scanning for the detection of defects within logs, *Bull. No. 8*, *Forest Research Institute*, New Zealand Service.

Burgess, A. E., 1985. Potential application of medical imaging techniques to wood products. In Szymani, R. (Ed.), *1st International Conference on Scanning Technology in Sawmilling*, October 10-12, San Francisco CA.

Birkeland, R., and Holoyen, S., 1987. Industrial methods for internal scanning of log defects: a progress report on an ongoing project in Norway. In Szymani, R. (Ed.), *2nd International Conference on Scanning Technology in Sawmilling*, October 1-2, Oakland/Berkeley Hills CA.

Chang, S. J., Olson, J. R., and Wang, P. C., 1989. NMR Imaging of internal features in wood. *Forest Products Journal*, Vol. 39, No. 1: pp. 43-49.

Cown, D. J., and Clement, B. C., 1983. A wood densitometer using direct scanning with x-rays. *Wood Science Technology*, Vol. 17. No. 2: pp. 91-99.

Davis, J.R, and Wells, P., 1992. Computed tomography measurements on wood. *Industrial Metrology*, Vol. 2: pp. 195-218.

Grönlund, A., 1992. Benefits from knowing the interior of the log. In Lindgren, O. (Ed.), *1st International Seminar on Scanning Technology and Image Processing on Wood*, August 30-September 1, Skellefteå Sweden.

Grundberg, S., and Grönlund, A., 1992, Log scanning – extraction of knot geometry. In Lindgren, O. (Ed.), *1st International Seminar on Scanning Technology and Image Processing on Wood,* August 30-September 1, Skellefteå Sweden.

Haralick, R. M., Sternberg, S. R., and Zhuang, X., 1987. Image analysis using mathematical morphology, *IEEE Trans. Pattern Analysis and Machine Intelligence,* Vol. PAMI-9. No. 4: pp. 532-550.

Harless, T. E. G., Wagner, F. G., Steele, P. H., Taylor, F. W., Yadama, V., and McMillin, C. W., 1991. Methodology for locating defects within hardwood logs and determining their impact on lumber-value yield, *Forest Products Journal,* Vol. 41, No. 4: pp. 25-30.

Hodges, D. G., Anderson, W. C., and McMillin, C. W., 1990. The economic potential of CT scanners for hardwood sawmills. *Forest Products Journal,* Vol. 40, No. 3: pp. 65-69.

Hopkins, F., Morgan, I. L., Ellinger, H., and Klinksiek, R., 1982. Tomographic image analysis. *Material Evaluation*, Vol. 40., No. 20: pp. 1226-1228.

Lantuéjoul, C., 1980. Skeletonization in quantitative metallography. In Haralick, R. M., and Simon, S.C (Eds.), *Issues of Digital Image Processing,* Sijthoff and Noordhoff, Groningen, The Netherlands.

Li, P., Abbott, A. L., and Schmoldt, D. L., 1996. Automated analysis of CT images for the inspection of hardwood logs. In *Proceedings of the 1996 IEEE International Conference on Neural Networks*, Washington, D.C.

Matheron, G., 1975. *Random sets and integral geometry.* New York: John Wiley.

Occeña, L. G., 1991. Computer integrated manufacturing issues related to the hardwood log sawmill. *Journal of Forest Engineering,* Vol. 3, No. 1: pp. 39-45.

Serra, J., 1982. *Image analysis and mathematical morphology.* London: Academic Press.

Schmoldt, D.L., 1996. CT imaging, data reduction, and visualization of hardwood logs. In Meyer, D. (Ed.), *Proceedings of the 1996 Hardwood Research Symposium*, Memphis, TN, pp. 69-80.

Schmoldt, D.L., He, J., and Abbott, A.L., 2000. Automated labeling of log features in CT imagery of multiple hardwood species. *Wood and Fiber Science* (in press).

Schmoldt, D. L., Li, P., and Abbott, A. L., 1997. Machine vision using artificial neural networks and 3D pixel neighborhoods, *Computers and Electronics in Agriculture,* Vol. 16, No. 3: pp. 255-271.

Soille, P., 1998. *Morphological Image Analysis*. Berlin: Springer-Verlag.

Taylor, F. W., Wagner, J. F. G., McMillin, C. W., Morgan, I. L., and Hopkins, F. F., 1984. Locating knots by industrial tomography – a feasibility study. *Forest Products Journal,* Vol. 34, No. 5: pp. 42-46.

Wagner, F. G., Taylor, F. W., Ladd, D. S., McMillin, C. W., and Roder, F. L., 1989. Ultrafast CT scanning of a oak log for internal defects. *Forest Products Journal,* Vol. 39.

Zhu, D. P., 1993. A feasibility study on using CT image analysis for hardwood log inspection. *Ph.D. dissertation*, Bradley Department of Electrical Engineering, Virginia Tech.

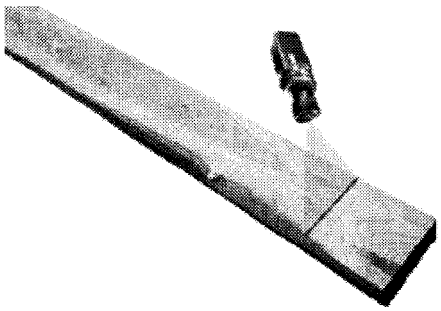

Proceedings:

4th International Conference on Image Processing and Scanning of Wood

IPSW 2000

21-23 August, 2000
Mountain Lake Resort
Mountain Lake, Virginia USA

D. Earl Kline and A. Lynn Abbott
Technical Editors

Sponsored by the USDA Forest Service, Southern Research Station
in cooperation with Virginia Polytechnic Institute and State University (Virginia Tech)
and the International Union of Forestry Research Organizations (IUFRO)